Geophys. J. R. astr. Soc. (1974) **39**, 361-383.

The Interpretation of Lava Flow Morphology

G. Hulme

(Received 1974 January 28)

Summary

It is postulated that lavas are non-Newtonian liquids with a yield stress and that it is the yield stress which determines flow dimensions. An appropriate theory was developed for the unconfined flow of ideal Bingham liquids on inclined planes. The occurrence of structures similar to levées on lava flows was predicted. The theory was verified by laboratory measurements on flows of suspensions of kaolin. These flows showed similarities to lava flows. Data from lava flows was also found to be in general agreement with the theory which was then used to interpret the shapes of two lunar lava flows. It was possible to estimate yield stresses and flow rates for these lavas.

1. Effects limiting the flow of lava

Lava flows show great variations in size, shape and surface features. The final form of a flow must be determined by the physical properties of the lava, its temperature and rate of extrusion and local conditions such as gravitational field strength and topography. The aim of the work presented in this paper is to isolate the parameters which have the greatest effect on flow morphology and to elucidate the relationship between the conditions at the start of a flow and the final form of the flow. At present there is no detailed knowledge of this kind but, were it available, the value of air- and satellite-photographs of lava flows would be greatly enhanced.

The hypothesis on which this work is based is that flowing lava is a non-Newtonian liquid and it is its non-Newtonian properties which are mainly responsible for the shapes of flows.

If lava were an ideal Newtonian liquid it would flow downhill and would continue to flow even after the supply at the vent had ceased until it ponded in a depression. Furthermore the flow would spread laterally until it was restricted by topography or until surface tension prevented spreading by which time it would be extremely thin. Observations show that lava does not behave like this. Commonly it comes to rest on a slope as soon as the supply of fresh lava ceases and many flow fronts are high and steep although unconfined by topographic features. It is clear that there is some process which limits the flow of lava, brings it to rest on slopes and prevents its lateral spreading.

The most obvious and apparently generally accepted process is the solidification of lava due to cooling. For this to be a feasible process the time taken for the development of a strong enough skin to prevent lateral motion must be realistic. The solid skin of a flow experiences an outward force due to the hydrostatic pressure of the lava and this must be balanced by an inward force which is the result of tension in the curved skin. If the skin can withstand the tension the lava will not flow laterally.

Assuming that the radius of curvature of the skin is about equal to the depth of the flow this condition is met when

$$s = \frac{g\rho d^2}{2S_T}$$

(A list of symbols appears at the end of this paper). The thickness of the cool skin increases with time according to

$$s = (8\kappa t)^{1/2}$$

(Ozisik 1968) and so the time needed to form a skin thick enough to prevent lateral flow is

$$t = (g\rho/S_T)^2 d^4/8\kappa.$$

It is seen that this time is proportional to the fourth power of the flow depth and so time increases rapidly with increasing depth of flow. If the tensile strength is that of cold, unfractured rock the time taken to halt a flow 1 m thick is less than half a minute but for a flow 8 m thick it is more than one day. This is far longer than the time it usually takes for the width of such a flow to become fixed. It is very unlikely that the tensile strength of the skin will be as great as that of cold rock both because some of the skin is very hot and because there are usually many cracks in the surface of a flow. It is doubtful whether a skin of freshly cooled lava has any appreciable tensile strength at the relevant length scale. It can be concluded that the surface cooling of lava flows is important only for small scale phenomena or after long time intervals. It may prevent the lava front flowing more than a certain distance from the vent but generally cannot prevent either lateral or downhill movement at any other point along the flow.

The part of a flow relatively near the vent may therefore be considered as isothermal because of the slow cooling rate and the small effect of a solid skin on the movement of lava. Yet even this part of a flow acquires a fixed depth and width soon after the commencement of activity. This may be explained if the rheological properties of lava are other than those of a Newtonian liquid.

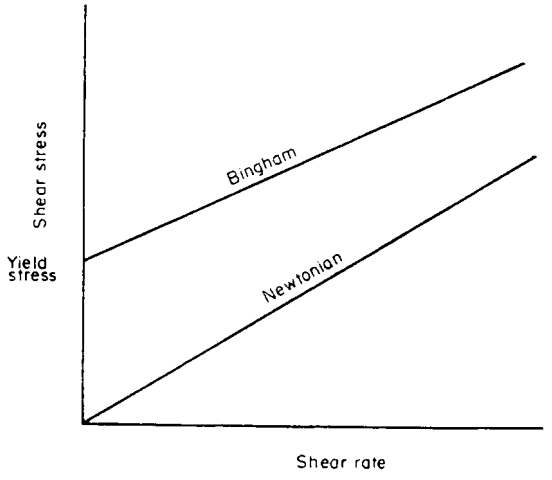

FIG. 1. Stress versus rate of strain for Newtonian and Bingham liquids.

Shaw *et al* (1968) measured the viscosity of a stationary lava and found that it showed non-Newtonian behaviour similar to that of a Bingham liquid. This idea is further discussed in Shaw (1969). The respective relationships between stress and rate of strain for Bingham and Newtonian liquids are shown in Fig. 1. The salient property of a Bingham liquid is that for stresses less than a certain value, the yield stress, the rate of strain is zero. The characteristic equation for a Bingham liquid is

$$S - S_y = \frac{\partial u}{\eta \partial z} \tag{1}$$

η is the gradient of the line in Fig. 1 and has the dimensions of viscosity. Here it will be called the plastic viscosity.

This paper is an attempt to show that the shapes of lava flows may be accounted for if it is assumed that lava behaves primarily as an isothermal Bingham liquid.

2. The free flow of Bingham liquid on a slope

In order to show that lava behaves as a Bingham liquid it is first necessary to investigate the behaviour of Bingham liquids in conditions similar to those in which lava flows are created. The simplest situation is that in which liquid is supplied from a small source on to an extensive inclined plane. Before any liquid issues from the source there is nothing on the plane which will define the width and depth of a flow. These characteristics must therefore depend completely on parameters such as the rate of supply, the properties of the liquid and the slope of the plane. The problem is to discover the nature of this dependence.

It is useful to consider the flow of Bingham liquids in pipes and between parallel plates for which equations are known (Skelland 1967). For flow in a pipe

$$F = \frac{\pi D^3}{32\eta} S_w \left[1 - \frac{4}{3}\left(\frac{S_y}{S_w}\right) + \frac{1}{3}\left(\frac{S_y}{S_w}\right)^4\right] \tag{2}$$

and between parallel plates

$$Q = \frac{h^2 S_w}{6\eta} \left[1 - \frac{3}{2}\left(\frac{S_y}{S_w}\right) + \frac{1}{2}\left(\frac{S_y}{S_w}\right)^3\right]. \tag{3}$$

S_w is the shear stress at the wall and is related to the dimensions of the flows as follows. In a pipe

$$S_w = \frac{GD}{4} \tag{4}$$

and between plates

$$S_w = \frac{Gh}{2} \tag{5}$$

where G is the pressure gradient driving the flow.

Substituting in equations (2) and (3) for the flow dimensions leads to

$$\frac{1}{2\pi} F\eta\, G^3/S_y^4 = \left(\frac{S_w}{S_y}\right)^4 - \frac{4}{3}\left(\frac{S_w}{S_y}\right)^3 + \frac{1}{3} \tag{6}$$

for pipe flow and

$$\frac{3}{2} Q\eta\, G^2/S_y^3 = \left(\frac{S_w}{S_y}\right)^3 - \frac{3}{2}\left(\frac{S_w}{S_y}\right)^2 + \frac{1}{2} \tag{7}$$

between parallel plates.

Equations (6) and (7) have the general form

$$\mathscr{F} = f(\mathrm{Y}) \tag{8}$$

where $\mathscr{F}$ is a dimensionless quantity relating flow rate to liquid properties and external forces. It has the important property that it is independent of the dimensions of the flow. Y is the dimensionless ratio of wall shear stress to the yield stress of the liquid. In effect it relates flow dimensions to liquid properties and external forces.

In the case of the free flow of a Bingham liquid on a plane the flow dimensions and wall shear stress are not defined initially. However they can only depend on the quantities on the left-hand side of equation (6) and so an equation of the same form as equation (8) will hold in this case also. This equation is the required relationship between flow dimensions and what may be called the initial conditions.

Naturally a more specific form of this equation is required. To this end it is helpful to consider how the width of the flow is determined. The lateral flow is driven by the pressure gradient due to the variation of flow depth across the flow. The lateral flow is thus similar to flow between parallel plates and is governed by a modification of equation (7). The important point is that the flow ceases when

$$S_w = S_y$$

S_w is given by

$$S_w = -g\rho\zeta \frac{\partial \zeta}{\partial y} \tag{9}$$

where ζ is the depth and y is the horizontal distance perpendicular to the direction of flow measured from the centreline of the flow. Lateral flow ceases and the transverse profile of the flow becomes fixed when

$$S_y = -g\rho\zeta \frac{\partial \zeta}{\partial y}. \tag{10}$$

The profile may be found by solving equation (10) with the condition that

$$y = w/2 \text{ at } \zeta = 0.$$

It follows that

$$\zeta^2 = \frac{2S_y}{g\rho}\left(\frac{w}{2} - y\right) \tag{11}$$

and the flow depth at the centreline is found by putting $y = 0$ whence

$$\zeta_o^2 = \frac{S_y w}{g\rho}. \tag{12}$$

The longtitudinal flow rate will also be zero when $S_w = S_y$. In this case, assuming flow depth to be constant along the flow,

$$S_w = g\rho \sin \alpha \zeta$$

and for small inclinations of the surface this may be written

$$S_w = g\ \rho\alpha\zeta. \tag{13}$$

Therefore, if the depth of the flow is less than a critical depth ζ_s there will be no downhill movement. ζ_s is given by

$$\zeta_s = S_y/g\rho\alpha. \tag{14}$$

This implies that there will be a region along each side of the flow, where the depth is

less than ζ_s, where there will be no longitudinal flow. The edge of this region may be found by putting $\zeta = \zeta_s$ in equation (11). If y_s is the distance from the centreline at which the critical depth is reached (Fig. 2) then

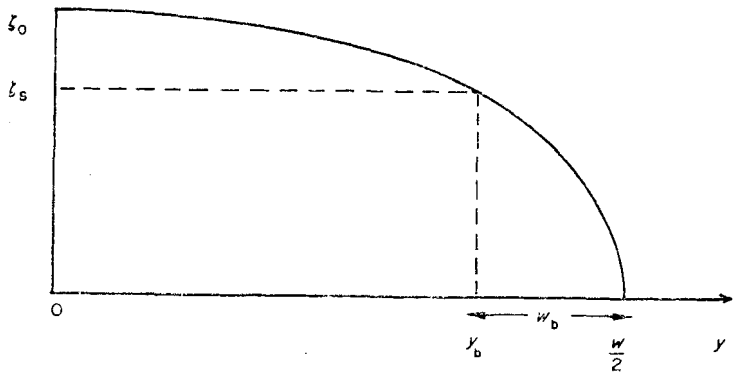

FIG. 2. Diagram of flow profile.

$$y_s = w/2 - w_b \tag{15}$$

where w_b is the width of the region of stationary liquid and is given by

$$w_b = \frac{g\rho\zeta_s^2}{2S_y} . \tag{16}$$

Substituting from equation (14) leads to

$$w_b = \frac{S_y}{2g\rho a^2} = \frac{\zeta_s}{2a} . \tag{17}$$

The flow rate may be expressed as

$$F = \int_{-w/2}^{w/2} Q \, dy = 2 \int_0^{w/2} Q \, dy .$$

Since there is no flow beyond $y = y_s$ this is equivalent to

$$F = 2 \int_0^{y_s} Q \, dy. \tag{18}$$

If the flow is much wider than it is deep then Q may be calculated approximately from equation (3). The flux per unit width in a flow of depth ζ on a plane is half that in a flow between parallel plates of separation 2ζ. Hence

$$Q = \frac{\zeta^2}{3\eta} S_w \left[1 - \frac{3}{2}\frac{S_y}{S_w} + \frac{1}{2}\left(\frac{S_y}{S_w}\right)^3\right]$$

Substituting from equations (13) and (14) gives

$$Q = \frac{g\rho a\zeta_s^3}{3\eta} \left[\left(\frac{\zeta}{\zeta_s}\right)^3 - \frac{3}{2}\left(\frac{\zeta}{\zeta_s}\right)^2 + \frac{1}{2}\right] . \tag{19}$$

Hence

$$F = \frac{2}{3}\frac{g\rho a\zeta_s^3}{\eta} \int_0^{y_s} \left[\left(\frac{\zeta}{\zeta_s}\right)^3 - \frac{3}{2}\left(\frac{\zeta}{\zeta_s}\right)^2 + \frac{1}{2}\right] dy \tag{20}$$

and integration gives

$$F = \frac{g\rho\zeta_s^4}{\eta} \left[\frac{2}{15}\left(\frac{\zeta_0}{\zeta_s}\right)^5 - \frac{1}{4}\left(\frac{\zeta_0}{\zeta_s}\right)^4 + \frac{1}{6}\left(\frac{\zeta_0}{\zeta_s}\right)^2 - \frac{1}{20}\right] . \tag{21}$$

From equations (13) and (14)

$$\frac{\zeta_o}{\zeta_s} = \frac{S_w}{S_y} \text{ at the centreline.}$$

Equation (21) is therefore a specific form of equation (8) for the case of the free flow of a Bingham liquid on a plane. It must be remembered that equation (21) is only an approximation because of the approximate method by which F was calculated. Agreement with reality will improve as the flow width increases with respect to flow depth.

The quantities $\mathscr{F}$ and Y may now be defined explicitly. They are

$$\mathscr{F} = F\eta/g\rho\zeta_s^4 \tag{22}$$

which in terms of initial conditions is

$$\mathscr{F} = F\eta\,(g\rho)^3 \left(\frac{a}{S_y}\right)^4 \tag{23}$$

and

$$Y = \frac{g\rho a\zeta_o}{S_y}. \tag{24}$$

Y is thus a dimensionless form of the centreline depth of the flow. ζ_o is not a particularly useful quantity because it is very difficult to measure on real lava flows. More useful is the flow width which can be easily measured from photographs. Equation (12) allows Y to be expressed in terms of w whence

$$Y = \left(\frac{g\rho a^2}{S_y}\right)^{1/2} w^{1/2}.$$

Substituting from equation (17) leads to

$$Y = \left(\frac{w}{2w_b}\right)^{1/2}. \tag{25}$$

For convenience the quantity Y is replaced by another dimensionless parameter W, where

$$W = Y^2 = \frac{w}{2w_b}. \tag{26}$$

Equation (21) then becomes

$$\mathscr{F} = \frac{2}{15} W^{5/2} - \frac{1}{4} W^2 + \frac{1}{6} W - \frac{1}{20}. \tag{27}$$

This equation may be tested experimentally and also with data from lava flows. Before making quantitative tests of the theory its value may be assessed by considering the qualitative predictions made so far. The major prediction is that regions of stationary liquid will develop along the sides of a flow. Such a phenomenon is in fact observed in the formation of levées along the sides of lava flows. Levées are very common features on lava flows (Fig. 3) and their mode of formation has not so far been satisfactorily explained. The fact that this simple analysis predicts the occurrence of structures similar to levées is striking confirmation that the hypothesis that lavas are primarily isothermal Bingham liquids is valid. The analysis also predicts that a flow will cease to spread laterally when it achieves a certain width and this width will be maintained as long as conditions do not change. This again is in accord with the behaviour of lava flows which commonly maintain an essentially constant width for great distances (Fig. 3, facing page 368).

3. Experimental investigation of the flow of the Bingham liquids on inclined planes

Experiments were carried out to test the analysis of the previous section. A search was made for a suitable liquid. No known liquid shows ideal Bingham behaviour but many have a yield stress. The liquid finally selected for use was a suspension of fine particles of kaolin in water. The suspension was convenient to make and its properties could be varied by altering the concentration of kaolin. The stress versus rate of strain curve was calculated for each sample used from measurements made with a Brookfield synchro-lectric rotating cylinder viscometer. A typical characteristic curve is shown in Fig. 4. The viscometer measurements were made first at increasing rotation rates and then at decreasing rotation rates. The results were slightly different and their mean was used to construct Fig. 4. This type of characteristic curve is commonly seen in suspensions like the one used here (Daum & den Otter 1971). The yield stress is usually taken to be where the backward extrapolation of the upper part of the curve intersects the stress axis but in fact some flow occurs at weaker stresses. A graph of yield stress against concentration of kaolin is shown in Fig. 5.

A diagram of the flow simulation apparatus is shown in Fig. 6. After preparation the properties of a kaolin suspension were measured and it was then transferred to the glass storage bottle. To produce a flow the suspension was extruded on to the inclined plane through a one-inch diameter pipe by pressure provided by water in the header

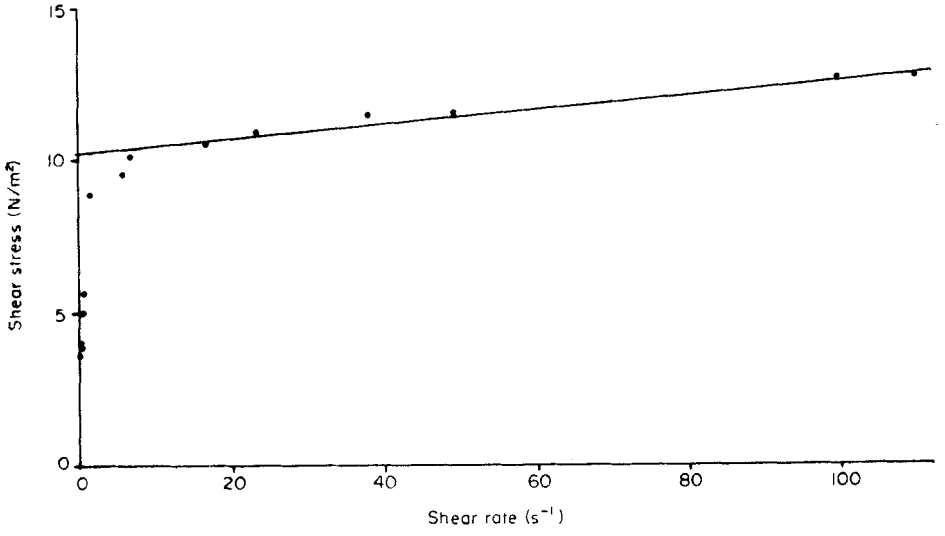

FIG. 4. Stress versus rate of strain for a kaolin suspension.

tank. The water was kept separate from the suspension by means of a plastic bag acting as a diaphragm in the entry to the bottle. The rate of flow was controlled by the tap. During each flow the rate of advance of the flow front was measured by timing its passage across lines spaced at 10-cm intervals along the plane. Flows typically lasted for about 5-min although one flow travelled 80 cm in under a minute, while another one took 5 h to travel less than 20 cm. The supply ceased when the bottle was emptied or when the tap was turned off and the flows always came to rest very shortly afterwards. Photographs were taken during and after flows and some are shown in Figs 7–9. It is seen that levées are formed, as predicted, and lateral spreading becomes very slow at small distances from the vent. Apparent fracture planes due to failure under shear stress are very common in the flows. These presumably occur when the shear rate is high enough for conditions to be represented by the upper part of the characteristic curve where plastic viscosity is very low. The sharp contrast in plastic

viscosity between upper and lower parts of the curve means that as shear rate increases the liquid will apparently suddenly begin to flow rapidly. This will occur in isolated parts of the liquid where the yield stress is slightly lower than elsewhere because once one part yields the shear stress is reduced in surrounding regions.

Measurements were made at several points along the stationary flows of total

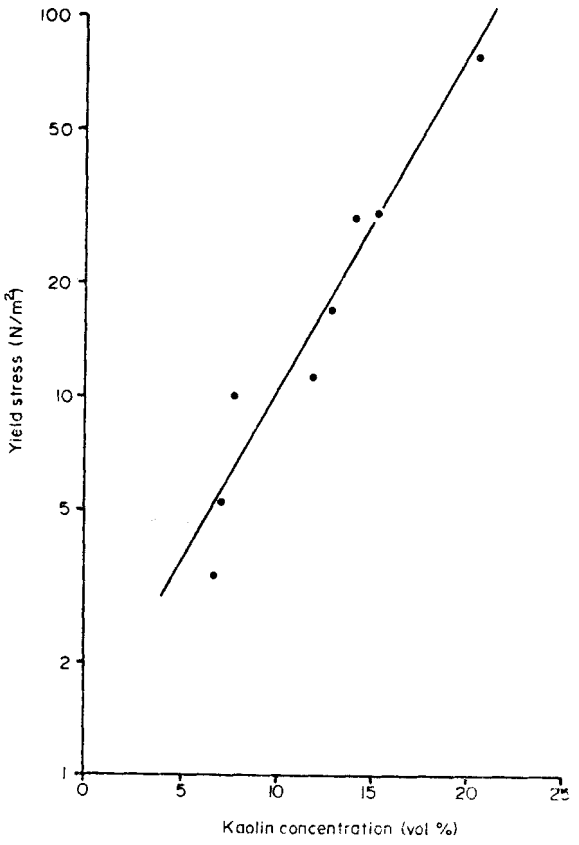

FIG. 5. Yield stress versus concentration of kaolin.

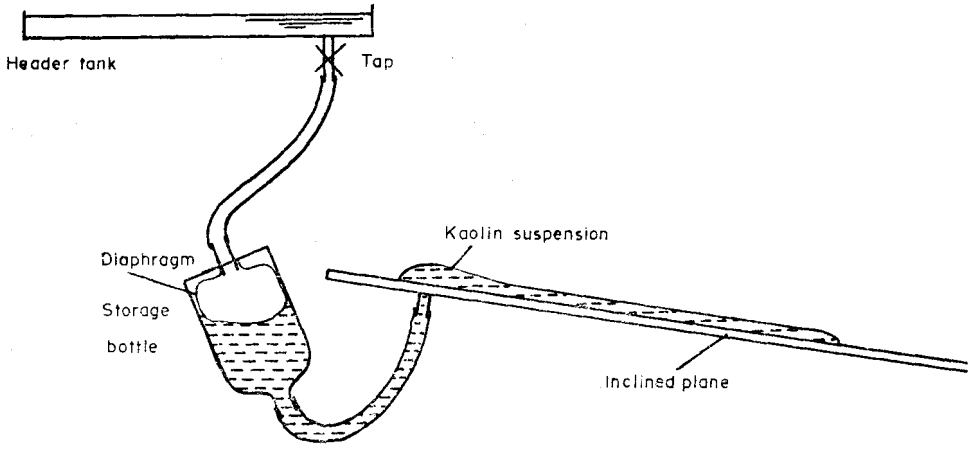

FIG. 6. Diagram of flow simulation apparatus.

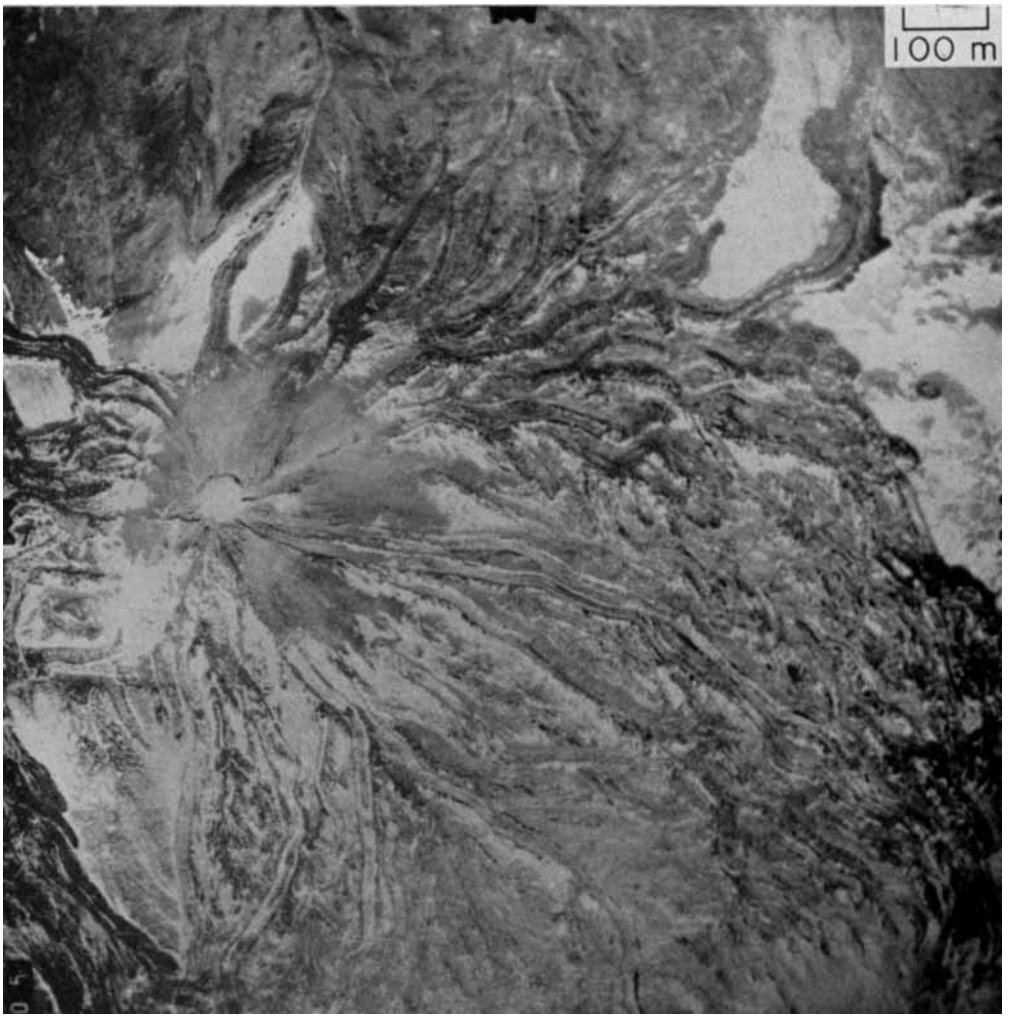

FIG. 3. Lava flows with levees, Teide, Tenerife. The slope of the cone is fairly uniform at about 30°. (By permission of Trabajos Fotofraficos Aereos S.A.).

facing p. 368

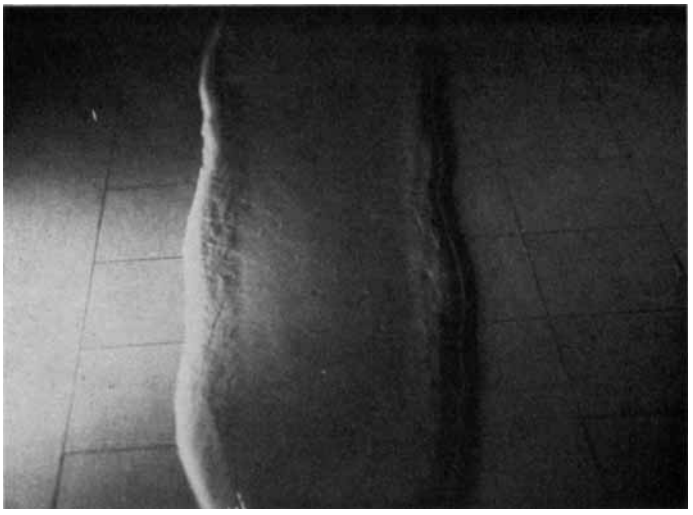

FIG. 7. Flow A.

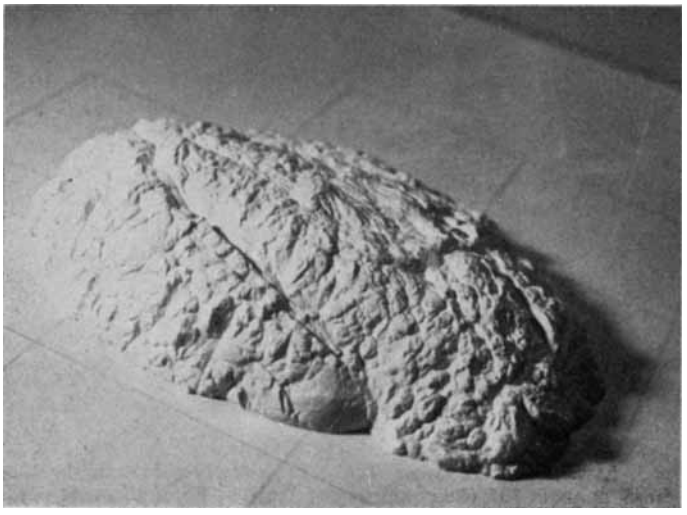

FIG. 8. Flow I.

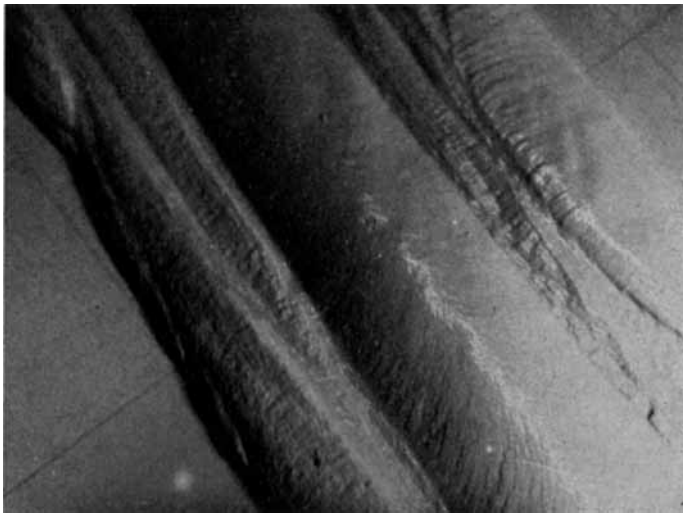

FIG. 9. Close-up of flow K.

Table 1

Data for laboratory flows

Flow	ρ (10^3 kg m^{-3})	S_y (N m^{-2})	η (Pa s)	α	u_m (mm s^{-1})	ξ_s (mm)	w (mm)	$2w_b$ (mm)	W	$\mathscr{F}$
A	1·12	5	1·8	0·144	2·6	3	87	21	8·2	2·83
B	1·13	10	3·7	0·159	2·4	6	240	39	6·7	1·50
C	1·11	3·3	1·2	0·111	3·7	3	350		14·2	13·4
D	1·23	29	12·2	0·195	2·8	12	250	48	4·1	0·50
E	1·23	29	12·2	0·219	4·6	11	240	72	4·8	1·00
F	1·25	30	9·0	0·207	0·64	12	250	43	4·3	0·080
G	1·25	30	9·0	0·227	0·9	11	200	39	4·1	0·123
H	1·25	30	9·0	0·262	4·4	9	160	32	4·7	1·00
I	1·34	78	20	0·314	0·018	19	170		1·48	0·00116
J	1·25	35	12	0·314	5·8	9	200		7·0	2·16
K	1·25	45	15	0·308	1·0	12	170	52	4·4	0·150

width, levée width, centreline depth and levée depth. Measurements were made far enough from the vent for conditions to have become steady. Towards the vent depth increases and width decreases. In this region the slope of the liquid surface contributes most of the pressure gradient. Further from the vent the surface of the liquid becomes flatter and the pressure gradient due to the slope of the plane is the dominant driving force. Here both flow width and depth become constant. The downstream distance beyond which conditions are constant may then be estimated by

$$x_c \sim \zeta_0/\alpha$$

and this was usually about 10 cm. Rods calibrated in millimetres were used for the measurements; these were accurate enough because natural variations in the quantities

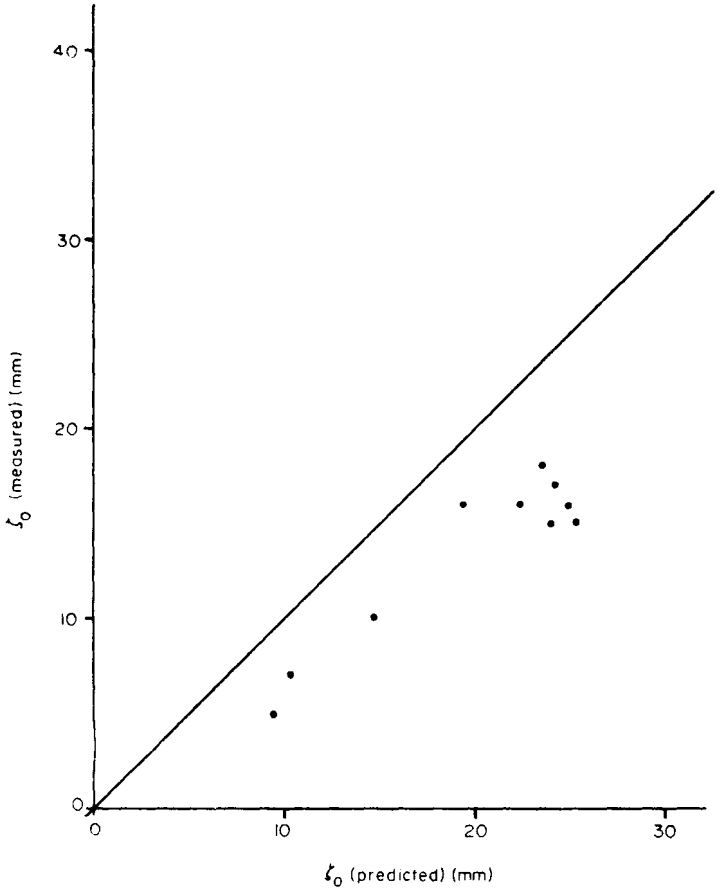

FIG. 10. Comparison of measured and predicted values of centreline depth.

to be measured were large as can be seen from the photographs. These fluctuations were probably caused by small inhomogeneities in the liquid and the resulting fluctuations in flow rate. Table 1 lists the relevant data for 11 flows.

The measurements were used to verify the equations of Section 2. Equation (14) was checked first. It was found that the value of S_y predicted by equation (14) using the measured value of ζ_s was always in good agreement with the value taken from the characteristic curve. The measured values of ζ_0 were then compared with the values predicted by equation (12). The results appear in Fig. 10 and it may be seen that ζ_0

was usually measured to be only about three-quarters of the predicted value. The anomalously high measured value of ζ_0 was from flow I which was a very short flow and measurements had to be made too close to the vent. The discrepancy between theory and experiment was not unexpected here because the profile given by equation (11) cannot be correct at the centreline where it implies a discontinuity in the surface curvature. The uncertainty in the value of ζ_0 is not important for the verification of equation (27).

Next the widths of the levées were compared with the prediction of equation (17). Fig. 11 shows a graph of $2w_b$ against ζ_s/α. There were several difficulties in measuring the width of levées. First their widths varied to some extent along a flow and some became vanishingly thin while new levées appeared. Several flows produced two or more sets of levées (Fig. 9) which possibly stemmed from fluctuations in flow rate. It was found that the outermost levées agreed best with predictions and in cases where

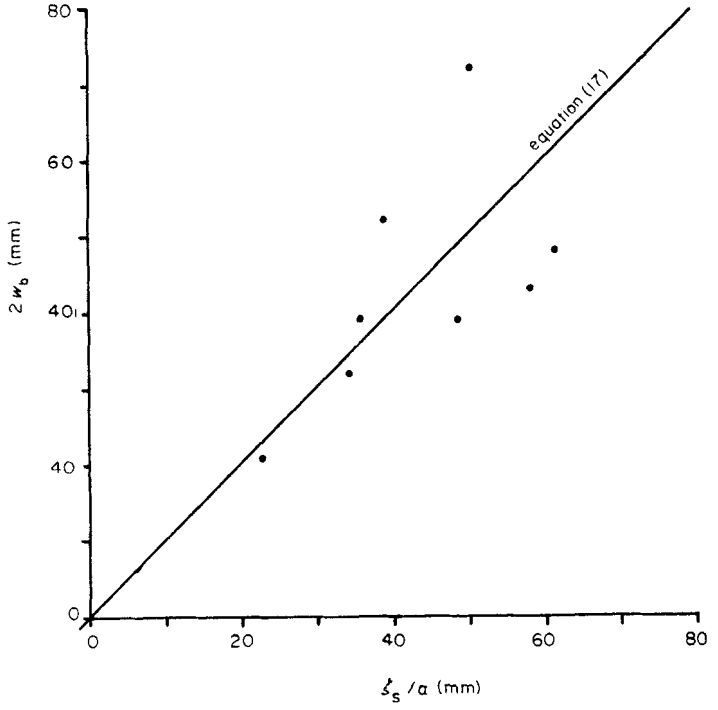

FIG. 11. Comparison of measured and predicted values of levée width.

several levées were present it was the outermost one which was used. For flows C, I and J it was not possible to make meaningful measurements. In spite of these difficulties—which account for the scatter on the graph—it seems reasonable to conclude that equation (17) is verified by the experiments. It was then possible to calculate W for each flow using

$$W = \frac{w\alpha}{\zeta_s}. \tag{28}$$

This equation was preferable to equation (26) because the quantities may be measured more accurately than levée widths.

To proceed further it was necessary to know the viscosity, η, of the kaolin–water suspension and because the suspension was not an ideal Bingham liquid with a unique value of η it was difficult to decide which was the correct value to use. To find the most

relevant value of η an attempt was made to calculate it from the measurements made on the flows. The apparent viscosity η_a, was first calculated using Jeffreys' (1925) formula for the two-dimensional laminar flow of liquid on an inclined plane. This gives

$$\eta_a = \frac{g\rho\alpha d^2}{3u_c} \tag{29}$$

where the depth d was taken as the mean depth of the flow between the levées and u_c as the mean velocity of advance of the heat front. The quantities d and u_c were calculated by integrating equation (11) and they are expressed by

$$d = \zeta_s \frac{2}{3}\left(1 + \frac{W}{(W^{1/2} + 1)}\right) \tag{30}$$

and

$$u_c = u_m \left(\frac{W^{3/2}}{(W^{3/2} - 1)}\right). \tag{31}$$

Now apparent viscosity is defined by

$$S = \eta_a \frac{\partial u}{\partial z}$$

and by using equation (1) it is found that

$$\eta = \eta_a (1 - W^{-1/2}). \tag{32}$$

Having determined W it was possible to calculate η from measurements made on the flows. In general it was found that η was close to the value given by the steepest portion of the characteristic curve. It therefore seems that the higher values of η dominate the flow and it was decided that the slope of the steepest section of the characteristic curve would be used as the relevant value of η. This was probably not always accurate but it was possible to be consistent and the quantity used was a measured one which was preferable to a value calculated by an approximate method.

The flow rate F was calculated from

$$F = u_m A$$

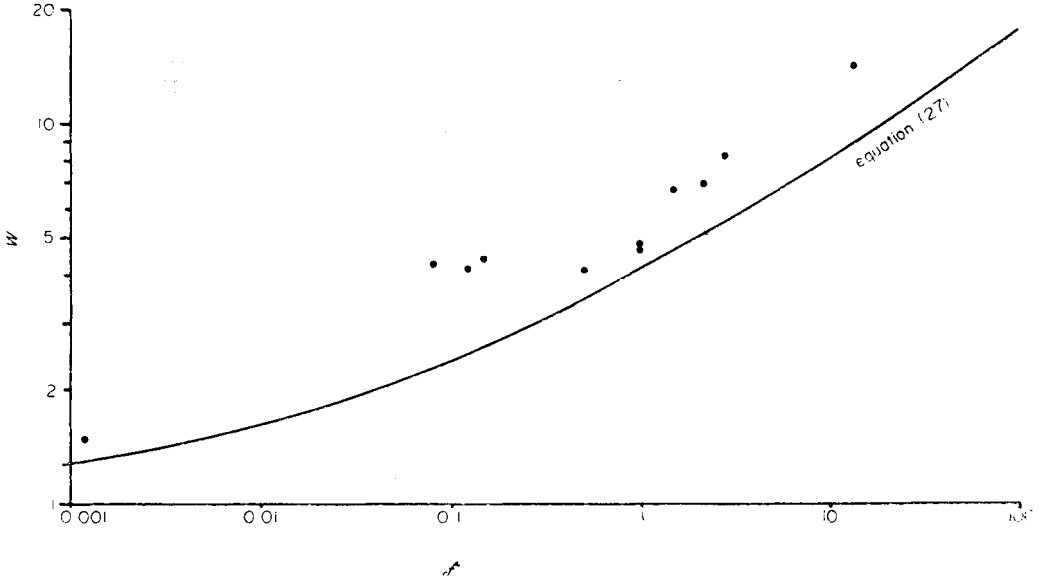

FIG. 12. $\mathscr{F}$ versus W. Experimental points compared with theory.

and the cross-sectional area, A was calculated by integrating equation (11). The result is that

$$F = (2/3)\,\zeta_s w u_m W^{1/2}. \tag{33}$$

It was then possible to evaluate $\mathscr{F}$ for each flow from equation (22) and the graph of $\mathscr{F}$ against W is compared with equation (27) in Fig. 12.

It can be seen that the experimental points all lie above the theoretical curve but the measurements are certainly of the same order as the predictions and show the same trend. The limited agreement between experiment and theory is all that could have been expected because of great uncertainties in experimental measurements. The greatest difficulty was presented by the determination of the relevant plastic viscosity for a liquid which was not an ideal Bingham liquid. This non-idealness of the liquid also means that the theory is not strictly applicable to it. Finally it must be recalled that the theory itself is only an approximation as described in Section 2.

In spite of these uncertainties the graph of Fig. 12 does show that the theory of Section 2 describes the free flow of Bingham type liquids accurately enough to be of use in the interpretation of lava flows. Furthermore, the experimental flows show similarities to lava flows in their behaviour: they develop levées, produce parallel-sided flows and cease flowing when the supply ceases.

4. Application of the theory to terrestrial lava flows

To test the hypothesis that lava flows are basically similar to those of Bingham fluids the relationship between dimensions and initial conditions of terrestrial flows was compared with that predicted by the theory of Section 2. It was difficult to find many flows for which sufficient data were available. There are many examples of flows with levées but for this comparison flow velocities were needed. This limited the choice to flows which had been observed while active. Among these there are very few for which all the required dimensions and flow rate have been measured. After some searching of the literature a total of four usable flows was found. Even then some of the data were very unreliable. The flows will be discussed individually.

Mauna Loa, 1942. Details of this flow were taken from Macdonald (1943). He reports a single estimate of flow depth of about 7 m at an unkown point on the flow approximately 24 km from the vent. The mean velocity is also given as from 90 to 150 m hr^{-1}. The slope of the ground was measured on a contour map of Hawaii and flow and levée widths were taken from air photographs at a point about 17 km from the vent. With this sketchy data it was possible to estimate both $\mathscr{F}$ and W. The total levée width was calculated from equation (17) and the value of 114 m was found to be significantly less than that of 260 m obtained from air photographs. The calculated value was the one used since this was more likely to represent the width of the original levées. The relevant data for all four flows are tabulated in Table 2.

Paricutin, 1945–6. There are just enough data for this flow in Krauskopf (1948) to allow $\mathscr{F}$ and W to be calculated independently. He gives a detailed map of the lower section of the flow from which slope and widths were taken. Several levées were built by the flow but only the outer ones may be used because they were presumably the first to be formed and so were unaffected by pre-existing levées. It was assumed that the flow was at its height when these levées formed and so the flow rate was taken to be at the upper end of the range reported by Krauskopf. Again flow depth was not well known. It is reported as being between 5 and 7 m at the lower ends of flows from Paricutin and so ζ_s was taken to be 6 m. The apparent viscosity of the flow was calculated as for the experimental flows by using equation (29). In the case of both Paricutin and Mauna Loa flows the results were higher than the generally quoted values of apparent viscosity (Walker 1973) but in each case they were representative of conditions much further from the vent than the points at which past estimates of viscosity were made. Plastic viscosity was calculated using equation (32).

Table 2

Data for lava flows

Flow	S_y (N m^{-2})	η (Pa s)	α	u_m (mm s^{-1})	u_c (mm s^{-1})	ξ_s (m)	w (m)	$2w_b$ (m)	F (m^3 s^{-1})	W	$\mathscr{F}$
Mauna Loa 1942	$8{\cdot}4 \times 10^3$	$1{\cdot}7 \times 10^5$	0·061	34	44	7	305	114	79	2·68	0·28
Paricutin 1945–6	$1{\cdot}3 \times 10^4$	$3{\cdot}6 \times 10^6$	0·11	3	3·5	6	210	55	5	3·82	0·71
Etna 1966	7×10^3	$1{\cdot}1 \times 10^3$	0·33	155	380	1·1	4·7	3·3	0·64	1·42	0·025
Etna 1966	7×10^3	$1{\cdot}5 \times 10^3$	0·20	38	200	1·8	10·4	9	0·51	1·15	0·0037

Underlined quantities are field observations or measurements from photographs.

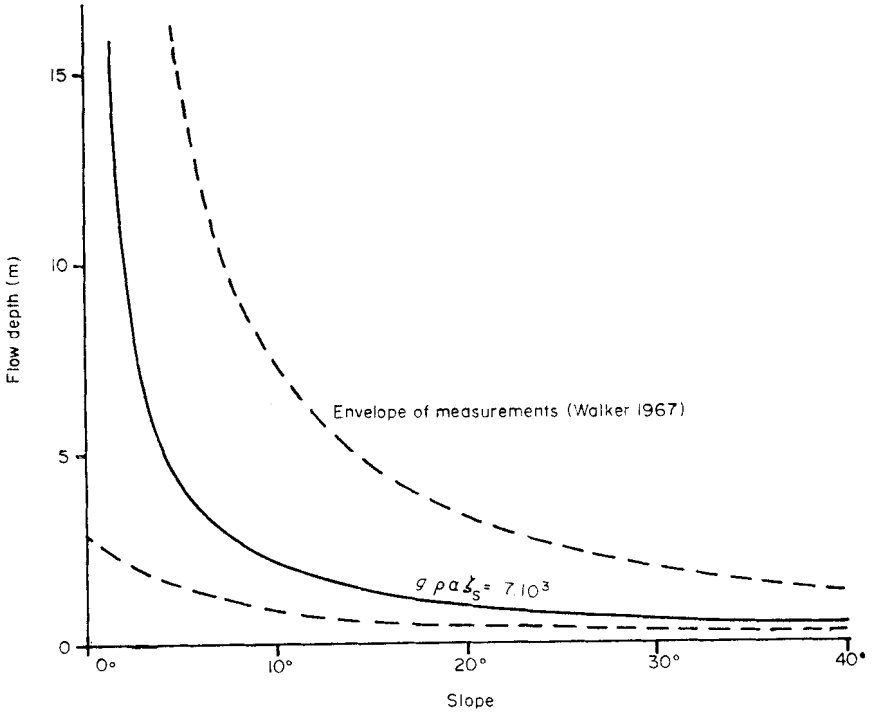

FIG. 13. Comparison of observed and theoretical relationships between flow depth and slope.

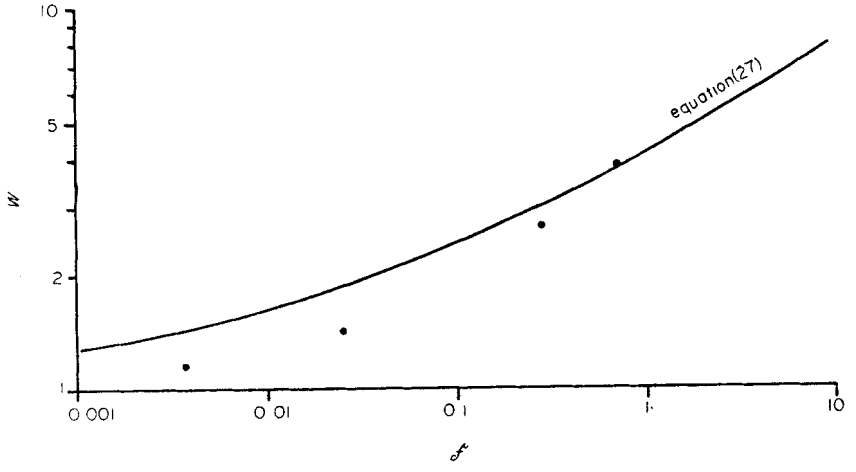

FIG. 14. $\mathscr{F}$ versus W. Field observations compared with theory.

Etna, 1966. Data for two flows were taken from Walker (1967). He plotted a graph of flow depth against slope. This relationship is predicted by equation (14) and is seen to depend on the yield stress of the lava. The predicted curve for a suitable value of S_y is shown superimposed on Walker's graph in Fig. 13. It is seen that equation (14) supported by observations. In fact it was Robson (1967) who first deduced from this data that Etnean lavas were Bingham liquids although this was not known to the present author at the time of the original writing. Consequently it is possible to achieve a good estimate of S_y for the Etnean lava. Approximate channel widths were

given by Walker but not levée widths. However equation (17) enabled these, and hence W, to be calculated. Apparent viscosity was estimated by Walker. His value is in close agreement with the value calculated in the same way as for the two previous flows. He also reported flow velocities and so approximate values of F could be calculated.

It is clear that the data for terrestrial flows are subject to much uncertainty. One quantity which was not measured for any of the four flows considered here is lava density. It was taken to be $2{\cdot}10^3$ kg m^{-3} throughout. Values for $\mathscr{F}$ and W were obtained for each of the four flows and compared with the predictions of equation (27). This is shown in Fig. 14. All the comments made about Fig. 12 apply equally to Fig. 14 but in spite of the many uncertainties observations made on terrestrial lava flows do seem to support the hypothesis that they are basically flows of isothermal Bingham liquids. This means that the shapes of lava flows may be interpreted with some confidence. Values of $\mathscr{F}$ may be predicted where values of W only are known from measurements made on air or satellite pictures. It also means that real flows may be modelled in the laboratory.

The yield stress of lava

There are several flows for which there are adequate data to allow the calculation of yield stresses of lavas. Equation (14) may be used if levée height, ground slope and lava density are known. For most terrestrial flows the value of W is low enough (that is, channels are relatively narrow) for the predicted centreline depth to be very little greater than the levée height. It is therefore acceptable to use flow depth as a measure of levée height. Very often, however, it is observed that levées are much higher than the surface of the flowing lava. This is at variance with the theory of Section 2 but it may possibly be explained as follows. The flow depth has obviously decreased since the levées were formed and this can happen, according to the theory, only if the yield stress of the lava has decreased. Such a decrease may be due to a change in composition of the lava but may also be due to a slight increase in its temperature because rheological properties are extremely temperate dependent.

Suppose that an increase in eruption rate were to occur. Then the mean velocity would be increased and the flow depth would tend to increase also. The increase in mean velocity would lead to a higher mean temperature at a particular point along the flow and this would reduce the yield stress, possibly by a large amount. The reduction in yield stress may then outweigh the increase in flow rate in its effect on flow depth and the paradoxical situation could arise where an increase in flow rate leads to a decrease in flow depth in a channel of fixed width. This effect could be looked for in the field.

It is commonly observed that levées grow by accretion. This will happen if lava on which blocks of solidified crust are floating overflows its levées owing to an increase

Table 3

Flow	Depth (m)	Slope	S_y (N m^{-2})	Reference
Oo-sima 1951	See text		$4{\cdot}3 \times 10^3$	Minakami & Sakuma (1953)
Tristan da Cunha	8	5°	$1{\cdot}4 \times 10^4$	Baker & Harris (1963)
Tristan da Cunha	14	10°	5×10^4	Baker & Harris (1963)
Hekla 1947	15	4°	2×10^4	Einarsson (1949)
Teide	8	30°	8×10^4	This paper
Etna	See text		7×10^3	Walker (1967)
Paricutin 1945–6	5	6°	$1{\cdot}3 \times 10^4$	Krauskopf (1948)
Mauna Loa 1942	7	3½°	8×10^3	Macdonald (1943)
Kilauea	See text		1×10^2	Shaw (1968)
Mare Imbrium	30	0·2°	4×10^2	Schaber (1973)

in flux. It is therefore probable that many levées are higher than predicted by the simple theory of Section 2 although their positions and widths may well be basically determined by the proposed mechanism.

Remembering that the simple theory cannot account for all the complexities of the real situation it is possible to estimate yield stresses for lavas which were effective at some stage of their flow. Table 3 gives details of ten determinations.

The data of Minakami were treated similarly to those of Walker for Etna. A graph of α against ζ was plotted and the best-fitting curve of the family

$$\alpha\, \zeta_s = \text{constant}$$

gave the value of S_y. The data for flows near the summit of Teide were obtained from measurements made on air photographs of Tenerife. Levée height was calculated from levée width according to equation (17). There was some difficulty in measuring levée width because of the effect of material slumping down the outside of the levées but it was possible to make a correction for this.

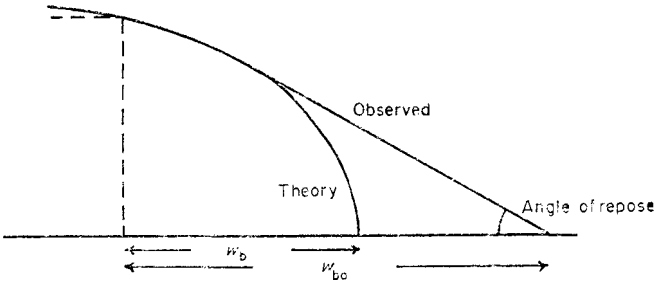

FIG. 15. Diagram of flow profile with slumping.

The theory indicates that the profile of a flow becomes vertical at the edges. Real flows do not have vertical walls (except perhaps pahoehoe flows) because, as is commonly observed, cooled blocks of lava continually fall off the walls. The profile stabilises when the surface of the fallen material achieves the angle of repose, θ_c, as shown in Fig. 15. The effect of this on levée width can be calculated easily and the true levée width is given in terms of the observed width, w_{bo}, by

$$w_b = w_{bo} \left\{1 + \left(\frac{\sin \alpha}{\tan \theta_c}\right)^2\right\}^{-1} \tag{34}$$

It can be seen that slumping causes a significant increase in levée width only when the slope of the ground is comparable with the angle of repose of unconsolidated blocks. The increase is only 10 per cent on a slope of 10° when the angle of repose is 30°.

The yield stress for Kilauean lava is the only one which has been measured directly (Shaw *et al.* 1968). This was done by sinking the head of a rotating cylinder viscometer in Makaopuhi lava lake. It would be expected that Kilauean lava would have properties similar to those of lava from Mauna Loa and the observed discrepancy in their yield stresses is probably due to the different temperatures at which the measurements were made. In the lava lake the temperature was close to the liquidus value whereas the yield stress for Mauna Loa lava was estimated at a point 17 km from the vent where the lava must have been very much below its liquidus temperature. It is probable that yield stress behaves similarly to viscosity in its dependence on temperature. The Mauna Loa lava yield stress would therefore be expected to be higher than that of the Kilauean lava and the difference between the two values is an indication of the variation of yield stress over the melting range of a lava.

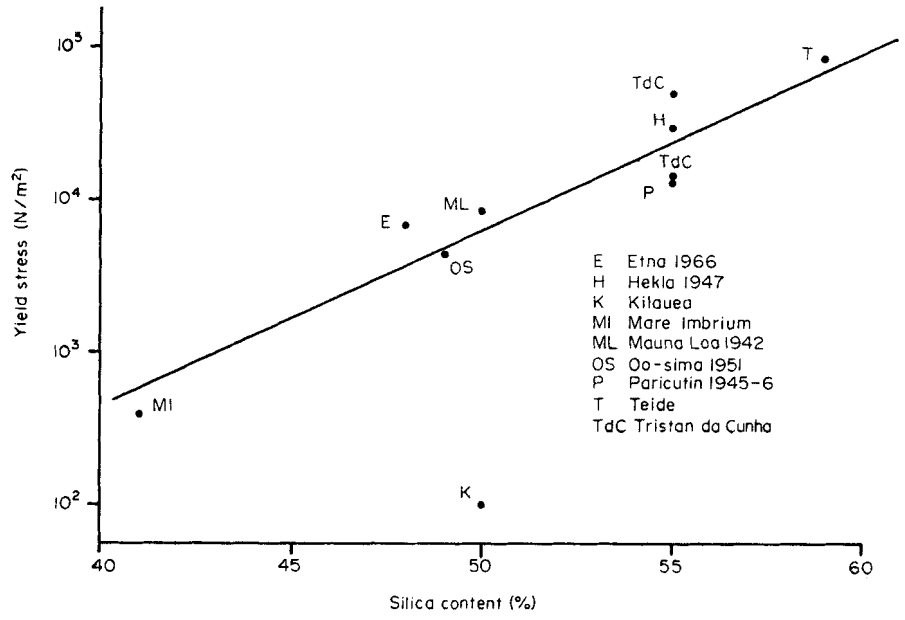

FIG. 16. Yield stress of lava versus silica content.

Yield stress was plotted (Fig. 16) against silica content of the lavas. Silica content was used to classify the lavas because it is known to be related to the rheology of lavas (Bottinga & Weill 1972). There are few points and a large amount of scatter due mainly to the lack of temperature control but in spite of this a trend of increasing yield stress with silica content may be seen. This is again similar to the variation of viscosity.

Pahoehoe and Aa Lava

The existence of a yield stress may also account for another commonly observed phenomenon of lava flows—the transition from pahoehoe to aa lava.

The surface of a liquid is kept smooth by the action of surface tension. If a normally plane liquid surface is distorted then surface tension forces act on the distorted region to restore the surface to a plane. The surface of flowing lava is continually being broken and distorted but if the lava possesses a yield stress then surface tension forces must overcome the yield stress before any smoothing of the surface takes place. For three-dimensional distortions with a radius of curvature R the condition for the distortion to be removed is

$$\frac{2T}{R} > S_y.$$

Hence for any lava there is a certain radius of curvature for distortions above which they will not be removed by surface tension. Therefore surface tension removes small scale perturbations of the surface but not large scale ones. The critical radius of curvature is

$$R_c = \frac{2T}{S_y}. \tag{35}$$

Therefore lavas of high yield stress and low surface tension will be able to sustain smaller scale surface distortions.

The surface tension of lavas has been measured in the laboratory (McBirney & Murase 1970) and it is found that, for all lavas, surface tension increases with in-

creasing temperature. Also, lavas with lower silica content have higher surface tensions. This means that lavas of low silica content at high temperature have the lowest yield stresses and highest values of surfaces tension. Both of these factors lead to a high value of R_c and so the surfaces of these lavas remain smooth up to large scales. This is characteristic of pahoehoe lava which should therefore occur in hotter, more basic lavas which is in accord with observations. Cooling such lavas increases their yield stress and lowers their surface tension and both of these changes are marked. They both cause R_c to become smaller and so R_c is extremely sensitive to temperature. When R_c falls to less than about 1 mm a lava surface becomes spiny which is characteristic of aa lava and the transition may be rapid. Aa lava therefore occurs in cooler lavas and in lavas of higher silica content.

The yield stress at which transition to aa lava occurs may be calculated from equation (35). The surface tension of basaltic lava at its liquidus temperature is about 0·35 N m^{-1}. Supposing that the transition occurs when R_c is 1 mm means that the yield stress must be 700 N m^{-2}. This value fits in well with those plotted in Fig. 16 where cool Hawaiian lava of aa type has S_y of order 10^4 N m^{-2} and Hawaiian lava close to its liquidus and of pahoehoe type has S_y of order 10^2 N m^{-2}.

Development of a lava flow

From the evidence that has been presented it is concluded that, to a first approximation, lava behaves like an isothermal Bingham liquid. This knowledge is very helpful when interpreting the shapes and dimensions of lava flows. The formation of a flow will now be described.

At the start of an effusive eruption there are basically six predetermined parameters which define the shape of the subsequent flow. These are the lava flux, the gravitational field strength, the slope and three lava properties—density, plastic viscosity and yield stress. The effects of temperature variations may be ignored in the first instance. These six parameters combine to form the dimensionless quantity $\mathscr{F}$ which characterises the flow. It is directly related in the way which has been described to the quantity W which relates the width and depth of the flow to the initial conditions. After flowing a short distance the flow achieves its predetermined width and depth which it maintains as long as conditions, in particular slope and effusion rate, stay constant. A flow automatically develops levées and in terrestrial flows the flow depth is never very much greater than the height of these levées. Levée height is therefore a good indication of flow depth and it is proportional to the yield stress of the lava. Yield stress increases with silica content and so basaltic lavas give rise to less deep flows than do more acidic lavas.

The ratio of flow depth to flow width may be called the aspect ratio. This is a very useful quantity for describing the shape of a flow. (See Appendix 1). A flow of low aspect ratio is wide and of small depth while a high aspect ratio flow is narrow and deep. Aspect ratio may be measured at any point along a flow and it will change as conditions change. If levée height is used to represent flow depth then, from equation (28),

$$\text{Aspect ratio} = \frac{\zeta_B}{w} = \frac{a}{W}. \tag{36}$$

Now in the range

$$1{\cdot}5 < W < 10$$

the relationship between $\mathscr{F}$ and W is approximately

$$\mathscr{F} = W^4$$

and so, using equation (23),

$$\text{Aspect ratio} = S_y/(F\eta)^{1/4}\,(g\rho)^{3/4}. \tag{37}$$

Aspect ratio therefore depends mainly on yield stress. This predicts that lavas of low yield stress such as basalts will give rise to flows to low aspect ratio and more acidic lavas will occur in high aspect ratio flows. This is in general agreement with field observations.

Often flows cross a change in slope and by considering the aspect ratio it is possible to see how flow width is affected. Aspect ratio is shown by equation (37) to be approximately independent of slope but flow depth must change according to equation (14). The result is that flow width is inversely proportional to slope. This agrees qualitatively with observations but it has not been possible to confirm it accurately because of a lack of data.

Aspect ratio is also predicted to be insensitive to changes in effusion rate but in reality the situation is more complicated because of the effect of temperature variations. A large increase in effusion rate would tend to widen a flow slightly but the lava may be confined if levées it has already constructed have cooled enough to have become fixed. Moreover, a change in effusion rate changes the temperature of the flowing lava at a particular station and this may change the yield stress by a large amount. It has already been mentioned that an increase in flux may result in a lowering of the level of lava in a channel. A reduction in effusion rate could result in the construction of new levées inside the old ones and this is commonly witnessed.

When the supply ceases flow in the channel may continue for a short time until the centreline depth falls below the critical depth for flow to occur. The flow then comes to rest although it is possibly still in a fluid state and it may be reactivated if the supply recommences or if another flow overrides it and thereby increases the shear stress at its base.

5. Interpretation of lunar lava flows

Some lunar lava flows display channels and levées and it is therefore possible to use the foregoing theory to discover the initial conditions which determined the shapes of those flows. Measurements of channel width and total flow width were made on a section of a flow in south-west Mare Imbrium (Fig. 17). W was calculated to be 1·2 which by equation (27) implied $\mathscr{F}$ equal to $3{\cdot}2\ 10^{-4}$. The viscosity of simulated lunar flood basalts has been measured in the laboratory (Murase & McBirney 1970) where the lavas were treated as Newtonian liquids and so it is uncertain how the measured values of viscosity relate to plastic viscosity. For the want of better information the plastic viscosity will be assumed to be of the same order as the liquidus viscosity and this is about 10 Pa s. The flow rate of the Mare Imbrium lava flow was then calculated to have been $8{\cdot}10^4$ m^3 s^{-1}. Such a large effusion rate is compatible with the great distance which the flow travelled (over 200 kn) in accordance with the work of Walker (1973). It is also consistent with the high effusion rates predicted for sinuous rille formation (Hulme 1973).

The mean velocity, the velocity of the flow front, was found to be 0·4 m s^{-1} (1·4 km hr^{-1}) while the velocity in the channel was estimated at 1·7 m s^{-1}; these both seem reasonable values. The flow would have been emplaced in about six days if the effusion rate had remained steady. The mean depth of the flow is about 30 m (Schaber 1973) and substituting this into equation (17) gives a value of 1/250 for the slope of the lunar surface which is consistent with satellite measurements. The yield stress of the lunar basalt was then calculated to be about 400 N m^{-2} which is consistent with its low silica content (Fig. 16).

A lunar flow of a different lava type with well-developed levées is to be found close to the crater Tycho (Fig. 18). W was measured to be 1·8 and the height of one of the levées was estimated by measuring the length of its shadow, to be 60 m. The slope of the ground was then found to be 0·088 (5°) which is in accord with the measurements of Turner (1970) who estimated the slope at the same distance from the rim of

FIG. 17. Lava flow in south-west Mare Imbrium.
The section on which measurements were made is between the lines (Portion of Apollo 15 metric 1156).

facing p. 380

FIG. 18. Lava flow with well-developed channel near Tycho. (Portion of Orbiter V 128 H_2).

Tycho to be between 2° and 6°. The yield stress of this lava was calculated to be $1{\cdot}7\ 10^4$ N m^{-2} which indicates that it has a higher silica content than the Mare Imbrium lava. Its plastic viscosity was assumed to be similar to that of terrestrial lavas of similar yield stress and so a value of 10^6 Pa s seemed reasonable. The flow rate was then estimated to have been 750 m^3 s^{-1}. The flow is about 20 km long and again these values are consistent with the work of Walker (1973). The mean velocity is found to have been very low at 0·012 m s^{-1} or 1 km per day and so the emplacement time seems to have been of the order of 20 days. This evidence suggests that, whereas this flow may have been triggered by the formation of Tycho, by impact, the lava is not simply splashout from the impact. It was probably supplied at a fairly steady rate for a long period compared with the time of formation of the crater. A similar conclusion was reached by Strom & Fielder (1970) who used completely independent (morphological and statistical) arguments.

6. Summary

It was argued that the cooling of lava is too slow a process to be important in determining the widths and depths of lava flows. It was postulated that most lavas behave similarly to Bingham liquids and that it is the existence of a yield stress which determines flow dimensions.

Details were given of an approximate theory for the unconfined flow of ideal Bingham liquids on inclined planes. Surprisingly the occurrence of levées was predicted. Experiments were carried out to test the theory and the results supported the theory but their significance was limited because the experimental liquid was not an ideal Bingham liquid. Nevertheless the formation of levées was observed and the flows showed other characteristics of lava flows. Data from lava flows were then compared with the theory. Again some measure of agreement was found but accurate verification of the theory was not possible because the rheological parameters of lava are very poorly known and the flow data were of poor quality and coverage.

The theory needs more confirmation to increase confidence in its use and this will involve measuring the rheological properties of different types of lava at various temperatures. A greater supply of good quality data from active flows is also required. Flow depths need to be measured particularly accurately and at various stations along a flow in conjunction with gradient and velocity measurements. The dimensions of levées and channels are essential.

The hypothesis that it is the non-Newtonian behaviour of lavas which chiefly determines the morphology of flows has been shown to be very fruitful. It produced a simple explanation for the occurrence of levées and channels and a way of predicting flow dimensions from initial conditions. The value of the hypothesis is that it now becomes possible to estimate flow rates, velocities and possibly lava types from simple measurements on high altitude photographs of lava flows. This was demonstrated for two lunar flows and there are other lunar and martian lava flows to which the method will be applied.

Acknowledgments

I wish to acknowledge the NERC sponsorship of this work which has carried out in the Department of Environmental Sciences at the University of Lancaster as part of the research programme of the Lunar and Planetary Unit.

Lunar and Planetary Unit,
Department of Environmental Sciences,
University of Lancaster,
Lancaster LA1 4YQ.

References

Baker, P. E. & Harris, P. G., 1963. Lava channels on Tristan da Cunha, *Geol. Mag.*, **100**, 345–350.

Bottinga, Y. & Weill, D., 1972. The viscosity of silicate magmatic liquids, *Am. J. Sci.*, **272**, 438–475.

Daum, U. & den Otter, J. L., 1971. Clay. Chap. 16 in *Elasticity, plasticity and structure of matter*, eds R. Houwink & H. K. De Decker, 3rd edn, Cambridge University Press.

Einarsson, T., 1949. The eruption of Hekla 1947–8; IV.3 The Flowing Lava, *Soc. Scientiarium Islandica, Reykjavik*, 70pp.

Hulme, G., 1973. Turbulent lava flow and the formation of lunar sinuous rilles. *Mod. Geol.* **4**, 107–117.

Krauskopf, K. B., 1948. Lava movement at Paricutin Volcano, Mexico, *Geol. Soc. Am. Bull.*, **59**, 1267–1284.

Macdonald, G. A., 1943. The 1942 eruption of Mauna Loa, Hawaii, *Am. J. Sci.*, **241**, 241–256.

McBirney, A. R. & Murase, T., 1970. Factors governing the formation of pyroclastic rocks, *Bull. Volcanol.*, **34**, 372–384.

Minakami, T. & Sakuma, S., 1953. Report on volcanic activities and volcanological studies concerning them in Japan during 1948–51, *Bull. Volcanol.*, **14**, 79–130.

Murase, T. & McBirney, A. R., 1970. Viscosity of lunar lavas, *Science*, **167**, 1491–1493.

Osizik, M. N., 1968. *Boundary value problems of heat conduction*, International Textbook Co., Scranton, Penn.

Robson, G. R., 1967. Thickness of Etnean lavas, *Nature*, **216**, 251–2.

Schaber, G. G., 1973. *Lava flows in Mare Imbrium*. Fourth Lunar Science Conference, Houston.

Shaw, H. R., 1969. Rheology of basalt in the melting range, *J. Petrol.*, **10**, 510–35.

Shaw, H. R., Wright, T. L., Peck, D. L. & Okamura, R., 1968. The viscosity of basaltic magma: an analysis of field measurements in Makaopuhi lava lake, Hawaii, *Am. J. Sci.*, **266**, 225–264.

Skelland, A. H. P., 1967. *Non-Newtonian flow and heat transfer*, John Wiley & Sons, Inc., New York, London, Sydney.

Strom, R. G. & Fielder, G., 1970. Multiphase eruptions associated with the lunar craters Tycho and Aristarchus, *Comm. L.P.L. No.* 150, **8**, 235–288.

Turner, R. J., 1970. The northeast rim of Tycho, *Comm. L.P.L. No.* 149, **8**, 203–234.

Walker, G. P. L., 1967. Thickness and viscosity of Etnean lavas, *Nature*, **213**, 484–485.

Walker, G. P. L., 1973. Lengths of lava flows. *Phil. Trans. R. Soc. London, A*, **274**, 107–118.

Appendix 1

Aspect ratio

The purpose of this appendix is to avoid confusion over the use of the term aspect ratio which is likely to be widely used in future when discussing lava flows. The definition used here is different to the one given by Walker (1973) and was purposely chosen to be so. Aspect ratio is a term used commonly in aerodynamics where it is the ratio of the height or length of an aerofoil blade or wing compared with the chord length or distance from leading to trailing edge. The problem is which lava flow dimension should be used as a reference length analogous to chord length. Because it is really flow height which is being described it seems reasonable to use flow width as the reference length whereupon aspect ratio becomes equal to height/width. This means that, while in aerodynamics aspect ratio is usually greater than unity, it will always be far less than unity for lava flows but it seems more straightforward to say that a high aspect ratio flow is high in relation to its width than that it is of high width compared with its height.

Notation

A	cross-sectional area,	u_m	mean velocity of flow,
d	mean depth of moving lava,	w	flow width,
D	diameter of pipe,	w_b	levée width,
f	function of,	W	dimensionless parameter defined in equation (26),
F	flow rate, $m^3\ s^{-1}$,		
$\mathscr{F}$	dimensionless parameter defined in equation (8),	x	downstream distance,
		y	cross-stream distance from centreline,
g	gravitational field strength,		
G	pressure gradient,	y_s	distance from centreline at which critical depth is reached,
h	separation of parallel plates,		
Q	flow rate per unit width, $m^2\ s^{-1}$	Y	dimensionless parameter defined in equation (8),
R	radius of curvature,		
R_c	critical radius of curvature,	z	vertical distance,
s	skin thickness,	α	gradient of ground,
S	shear stress,	η	plastic viscosity,
S_T	tensile strength,	η_a	apparent viscosity,
S_w	wall shear stress,	ζ	flow depth,
S_y	yield stress,	ζ_s	critical flow depth,
t	time,	ζ_o	centreline depth,
T	coefficient of surface tension,	κ	thermal diffusivity,
u	velocity,	ρ	density.
u_c	mean velocity in channel,		